



ISSN: 0095-8972 (Print) 1029-0389 (Online) Journal homepage: <http://www.tandfonline.com/loi/gcoo20>

Spin-state dynamics of a photochromic iron(II) complex and its immobilization on oxide surfaces via phenol anchors

Philipp Stock, Nicole Spintig, Juliane Scholz, Jan Dirk Epping, Christian Oelsner, Dennis Wiedemann, Andreas Grohmann & Gerald Hörner

To cite this article: Philipp Stock, Nicole Spintig, Juliane Scholz, Jan Dirk Epping, Christian Oelsner, Dennis Wiedemann, Andreas Grohmann & Gerald Hörner (2015) Spin-state dynamics of a photochromic iron(II) complex and its immobilization on oxide surfaces via phenol anchors, *Journal of Coordination Chemistry*, 68:17-18, 3099-3115, DOI: [10.1080/00958972.2015.1066778](https://doi.org/10.1080/00958972.2015.1066778)

To link to this article: <http://dx.doi.org/10.1080/00958972.2015.1066778>




View supplementary material 



Accepted author version posted online: 29 Jun 2015.
Published online: 24 Jul 2015.



Submit your article to this journal 



Article views: 67



View related articles 



View Crossmark data 

Spin-state dynamics of a photochromic iron(II) complex and its immobilization on oxide surfaces via phenol anchors

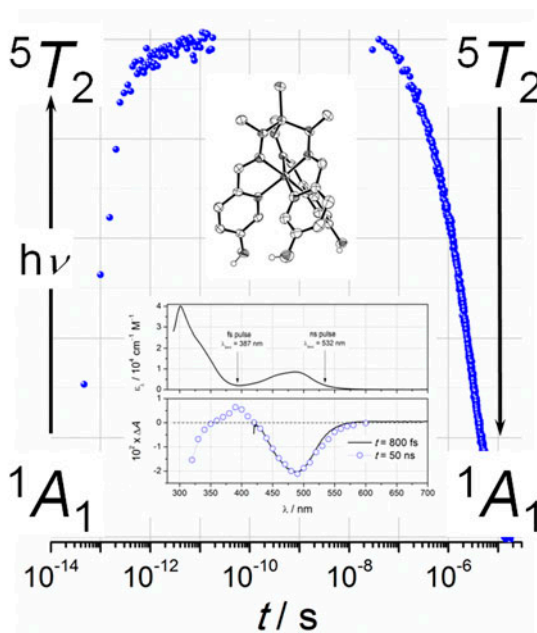
PHILIPP STOCK^{†‡}, NICOLE SPINTIG[†], JULIANE SCHOLZ[†], JAN DIRK EPPING[†], CHRISTIAN OELSNER[§], DENNIS WIEDEMANN[†], ANDREAS GROHMANN[†] and GERALD HÖRNER^{†*}

[†]Institut für Chemie, Technische Universität Berlin, Berlin, Germany

[‡]Department of Interface Chemistry and Surface Engineering, Max-Planck-Institut für Eisenforschung GmbH, Düsseldorf, Germany

[§]Department Chemie und Pharmazie, Friedrich-Alexander-Universität Erlangen-Nürnberg, Erlangen, Germany

(Received 17 March 2015; accepted 29 May 2015)



This work presents a detailed study of the photo-induced spin-state dynamics of the photochromic iron(II) complex **1**, where the metal ion is in the field of a tripodal hexa-imine ligand with protolysable phenol groups. The nature of the complex's ground state has been identified as a spin singlet by ¹H NMR and steady-state UV/vis spectroscopies, and its distorted octahedral structure was

*Corresponding author. Email: gerald.hoerner@tu-berlin.de

Dedicated to Professor Rudi van Eldik on the occasion of his 70th birthday.

analyzed via crystal structure determination. Sub-picosecond and nanosecond time-resolved laser flash photolysis experiments identify the long-lived quintet state of **1** as the selective product of photoexcitation in the UV/vis spectral region. Thermal barriers of spin-state interconversion as a function of solvent and added base are derived from temperature-dependent rates of transient decay. Ground-state recovery is found to be significantly affected by the solvent and is strongly enhanced, in particular, by base-driven solvolysis of the ligand's phenol groups. Partial spontaneous deprotonation of the phenolic hydroxyl groups of **1** seems to prevail on metal oxide surfaces, *i.e.* on alumina. Composite materials, like **1** at Al_2O_3 , that retain the characteristic spectral features of the parent iron (II) complex can be readily obtained by wet impregnation of hydrous alumina with solutions of **1**.

Keywords: Spin crossover; Laser flash photolysis; Photophysics; Responsive surfaces; Phenols; Hydrogen bonding

1. Introduction

Many first-row transition metal complexes with a d^4 to d^7 electron configuration can undergo a stimulus-controlled transition between energetically close-lying spin states (spin crossover, SCO) [1, 2]. The most prominent example is SCO between the low-spin (LS; $^1A_{1g}/t_{2g}^6$, $S = 0$) and high-spin (HS; $^5T_{2g}/t_{2g}^4e_g^2$, $S = 2$) states in iron(II) complexes (d^6) in the bulk material [3, 4], where the discontinuous change of magnetic properties is accompanied by dramatic changes in visible-light response that can be selectively driven by visible light or effected by temperature gradients. The combined switching of magnetic and optical properties renders this class of compounds highly promising as opto-magnetic actors and sensors [1, 5–8].

Utilization of SCO on a molecular scale, that is, in isolated molecules, is hindered by the highly dynamic exchange among the spin states. An interesting recent access to trapped spin states relies on light-driven isomerization within the ligand sphere. Here, the spin state is altered via variation of the ligand field strength (light-driven ligand-induced spin change, LD-LISC [9, 10]) or variation of the ligand field symmetry (light-driven coordination-induced spin-state switching, LD-CISSS [11, 12]). Most commonly, however, it is only at

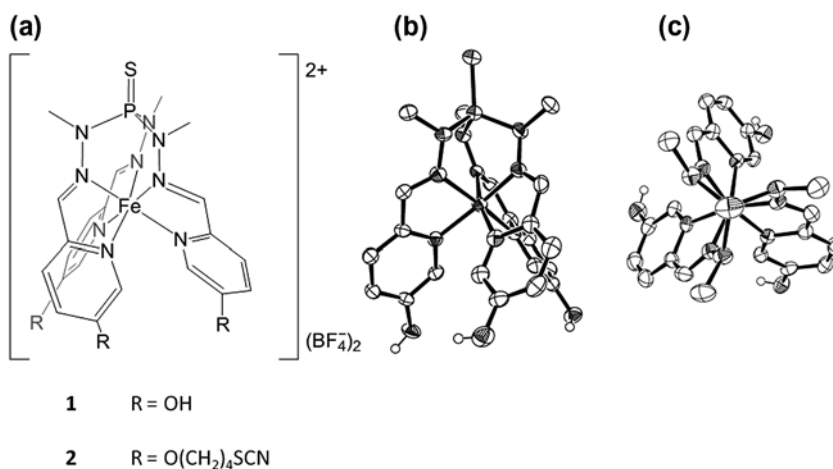


Figure 1. Chemical structure of **1** and **2** (a); single-crystal X-ray structure of the complex cation in **1** as viewed from the side (b) and along the pseudo-threefold axis (c). Ellipsoids at 50% probability, carbon-bound hydrogens are omitted for clarity.

cryogenic temperatures, where thermal barriers can effectively inhibit spin-state exchange (light-induced excited spin-state trapping, LIESST [13–16]).

In particular, at ambient temperature, very short quintet-state lifetimes, *i.e.* <1 ns, prevail for complexes of archetypal bidentate strong-field ligands such as bipyridine or phenanthroline [17, 18]. High-spin relaxation lifetimes $\tau_{1\leftarrow 5}$ for iron(II) complexes of multidentate ligands are only somewhat longer and typically fall in the range 50–150 ns [19–24]. Very recently, however, we provided clear-cut evidence that labile spin states can be stabilized kinetically by tuning the ligand topology. In particular, a family of iron(II) complexes of tripodal hexadentate N_6 ligands have spin-state lifetimes of up to 10 μ s at room temperature [25].

In order to gain deeper insight into the intramolecular and intermolecular parameters controlling the spin-state dynamics, we have selected from this family of extraordinary iron(II) complexes, *tris*-phenolic **1** and its phenol ether analog **2** as a reference (for structures, see figure 1) [26]. In this work, we present a detailed study of the structure and the photophysical properties of **1**. Steady-state and time-resolved UV/vis spectroscopies (sub-picosecond and nanosecond timescales) serve to characterize the photo-induced spin-state dynamics of **1** in solution with respect to solvent nature and degree of OH protolysis.

In a second section, we introduce a novel but straightforward method to immobilize functional metal complexes on metal oxide surfaces. We utilize the high affinity of hydrous metal oxide surfaces for the phenol groups [27] in order to immobilize the salt-like, hydroxypyridyl-bearing iron(II) complex **1** from solution. Composite materials are readily obtained via wet impregnation of alumina with **1** in acetone solution. This ready access to immobilized, *salt-like* metal complexes lifts the restriction to evaporation–deposition cycles (which, in any case, require *electroneutral* complexes). Notably, a few results reported for immobilized SCO molecular compounds on gold or pyrolytic carbon surfaces have so far relied almost exclusively on *electroneutral* iron(II) complexes [26, 28–35].

2. Experimental

Synthetic procedures and analytical data for the iron(II) complex **1** of the tripodal hexa-imine ligand **L** (**L**: tris(1-methyl-2-([5-(4-hydroxy)pyridin-2-yl]-methylene)hydrazinyl)phosphane sulfide) used in this study were reported recently [25]. The corresponding iron(II) complex $[\text{Fe}\{\text{trenpy}_3\}](\text{BF}_4)_2$ of the well-established hexa-imine ligand trenpy_3 (**tren**: tris-(2-aminoethyl)amine; Schiff base adduct obtained from the condensation of ‘tren’ with three equivalents of pyridine-2-carbaldehyde) served as a reference material for time-resolved measurements. Steady-state UV/vis spectra in solution were measured with a Varian Cary 50 spectrometer, equipped with a UV/vis quartz immersion probe (light path 1 mm, Hellma), in a home-built measuring cell. Diffuse reflectance UV/vis (DR-UV/vis) spectra were recorded on a two-beam spectrometer (V670, JASCO) using an integration sphere coated with barium sulfate. Powder samples were measured undiluted in the spectral region of 220–890 nm. Commercial magnesium oxide (ABCR, 99.95%) was used as reflectance standard for baseline correction. The DR-UV/vis spectra were transformed in to the Kubelka–Munk function, $F(R_\infty) = K/S$ (K : absorption coefficient; S : scattering coefficient) [36].

2.1. Crystal structure determination of 1·(C₂H₅)₂O·H₂O

Single crystals suitable for X-ray structure analysis were obtained via isothermal diffusion of diethyl ether into an acetonitrile solution of **1** at 273 K. Data were collected at 150.0(4) K using an Oxford Diffraction Xcalibur S diffractometer equipped with a goniometer in κ geometry, a Sapphire 3 CCD detector, and a graphite-monochromated Enhance Mo- K_{α} source ($\lambda = 0.71073$ Å). Diffraction images were integrated with CRYSTALISPRO [Agilent Technologies, CrysAlisPro Software System, Intelligent Data Collection and Processing Software for Small Molecule and Protein Crystallography, Agilent Technologies Ltd., Oxford, U.K. (2014)]. An analytical absorption correction using a multifaceted crystal model was performed [37]. Structures were solved with SHELXT-2014 using dual-space methods and refined with SHELXL-2014 against F_o^2 data using the full-matrix least-squares algorithm [38]. Due to problems with the beam stop mask, some lower index reflections had to be excluded from the refinement. Non-hydrogen atoms were refined anisotropically; carbon-borne hydrogen atoms were refined isotropically with standard riding models. Oxygen-borne hydrogen atoms were refined with restrained O–H distances of 0.84 Å and $U_{\text{iso}}(\text{H}) = 1.2 U_{\text{eq}}(\text{O})$. Additionally, 1,3-distance restraints were applied (1.82 Å for the phenolic hydroxyl groups and 1.37 Å for the water molecule). ORTEP 3 FOR WINDOWS [39]. Crystallographic details are summarized in table 1.

Table 1. Crystal structure data for 1·Et₂O·H₂O.

Empirical formula	C ₂₅ H ₃₆ B ₂ F ₈ FeN ₉ O ₅ PS
M_r	835.13
Crystal size (mm ³)	0.239 × 0.154 × 0.072
Crystal system	Triclinic
Space group	$P\bar{1}$
a (Å)	11.2468(19)
b (Å)	12.3413(19)
c (Å)	13.0831(14)
α (°)	80.847(12)
β (°)	84.466(12)
γ (°)	74.259(14)
V (Å ³)	1722.9(5)
Z	2
D_{calcd} (g cm ⁻³)	1.610
μ (cm ⁻¹)	0.639
$F(000)$ (e)	856
hkl range	−13 ≤ h ≤ 13 −15 ≤ k ≤ 15 −14 ≤ l ≤ 16
$([\sin \theta]/\lambda)_{\text{max}}$ (Å ⁻¹)	0.617
Refl. measured	14,087
Refl. unique (R_{int})	6752 (0.1019)
Refl. observed (R_{σ}) ^a	3750 (0.1658)
Param. refined/restr.	489/8
u^b	0.0233
R_1/wR_2^b (obs. refl.) ^a	0.0683/0.1018
R_1/wR_2^b (all refl.)	0.1348/0.1329
S/S'	0.992/0.992
$\Delta\rho_{\text{fin}}$ (max/min) (e Å ⁻³)	−0.445/0.088

^a $I > 2 \sigma(I)$.

^b $R_1 = \sum ||F_o| - |F_c|| / \sum |F_o|$, $wR_2 = [\sum w(F_o^2 - F_c^2)^2 / \sum wF_o^4]^{1/2}$, $w = [\sigma^2(F_o^2) + (uP)^2]^{-1}$ with $P = [\max(F_o^2, 0) + 2F_c^2]/3$.

2.2. Surface grafting of **1** on alumina

Alumina (2.1 g, activated, neutral, Brockmann I from ACROS) was suspended in acetone (5 mL). After addition of **1** as a solid (3.2 mg, 3.8 μmol), the suspension was allowed to stir for 30 min. During this period the color changed from orange to red. The suspension was filtered, washed with acetone, and dried in a vacuum. The obtained pink powder was characterized by DR-UV/vis spectroscopy and solid-state magic-angle spinning (MAS) ^{31}P -NMR spectroscopy. ^{31}P -MAS-NMR spectra were recorded on a Bruker Avance 400 spectrometer (^{31}P : 161.92 MHz) using a 4-mm double resonance HX MAS probe. Data collection used a 90° pulse with a relaxation delay of 60 s under an MAS rotation of 12 kHz. Spectra were referenced to 85% H_3PO_4 in aqueous solution using solid $\text{NH}_4\text{H}_2\text{PO}_4$ ($\delta = 0.81$ ppm) as a secondary reference.

2.3. Laser flash photolysis (LFP)

Nanosecond Laser flash photolysis (LFP) experiments were performed with the laser wavelength 532 or 355 nm of a Nd:YAG laser system, as described in detail elsewhere [40]. Transient decays were recorded at individual wavelengths by the step-scan method in the range 340–700 nm and obtained as the mean signals of eight pulses. Spectral resolution was in the range ± 5 nm. The temporal pulse duration of 8 ns with energy of 2–3 mJ per pulse was generally much shorter than the decay lifetimes of the transient signals, so that deconvolution was not required for kinetic analysis. Before each measurement, the solutions of **1** in high-purity methanol, acetonitrile, and water ($\text{OD}_{532} = 0.3$; concentrations of **1** and **2** in the range $2\text{--}4 \times 10^{-5}$ M) were rigorously deoxygenated by flushing with analytical grade argon for 20 min prior to measurement, under argon, in sealed quartz cuvettes. For data acquisition at variable temperatures, we used a temperature-controlled cell holder (Quantum Northwest, model TC 125). Femtosecond transient absorption studies were performed with an amplified Ti/sapphire laser system (Model CPA 2101, Clark-MXR Inc. – output: 775 nm, 1 kHz, and 150-fs pulse width) in the TAPPS [Transient Absorption Pump/Probe System]-Helios from Ultrafast Systems between 400 and 800 nm. Laser pulses of 387 nm by frequency doubling of 775 nm with a pulse energy of 200 nJ per pulse were used for excitation of diluted solutions of **1** in high-purity acetonitrile solution ($\text{OD}_{387} = 0.2$; [**1**] = $4\text{--}8 \times 10^{-5}$ M) in a 2-mm Quartz cuvette at ambient temperature 293(2) K.

3. Results and discussion

3.1. Solid-state structures

Synthetic procedures and analytical data for **1** [25] have been reported elsewhere. In brief, the combination of equimolar mixtures of iron(II) tetrafluoroborate hexahydrate and the thiophosphoryl-capped hexa-imine ligand **L** in methanol afforded deep red solutions of the complex ion. From these solutions, **1** was obtained as a red solid in good yield. **1** crystallizes in the space group $P\bar{1}$ with one helically chiral complex cation, two tetrafluoroborate anions, and one molecule each of diethyl ether and water in the asymmetric unit. Three phenolic hydroxyl groups of each complex donate hydrogen bonds to one tetrafluoroborate ion, the diethyl ether molecule, and the water molecule (see figure S1, see online supplemental material at <http://dx.doi.org/10.1080/00958972.2015.1066778>). The water

molecule, on the other hand, donates one hydrogen bond to each crystallographically independent tetrafluoroborate ion.

Coordination of the N₆ ligand to iron(II) affords a distorted octahedron (figure 1(b) and (c)). The appearance of the complex ions in **1** and their metrics largely resemble the data reported for the phenol ether analog **2** (table 2). N–Fe–N *cis*-bond angles of both compounds show little deviation from the ideal value of 90° (average deviation |Δ_{cis}| < 4°). Also, the three N–Fe–N *trans*-angles are commensurate with octahedral coordination. Their systematic and significant deviation from 180° (Δ_{trans} = 13°; table 2), however, indicates the action of a specific distortion mechanism. We ascribe this distortion to constraints brought about by the highly preorganized ligand backbone with its rigid P(S)N₃ capping unit. In agreement with this assignment, the trigonal twist angles θ (Bailar twist, [41]) of the [FeN₆] core deviate significantly from the ideal θ = 60° in the regular octahedron. In sum, the coordination sphere can be classified as octahedral with significant trigonal distortion along the pseudo-threefold symmetry axis as defined by the vector S–P–Fe. At this point, it is important to note that Breher *et al.* observed even more pronounced trigonal distortion after coordination of a very closely related hexa-imine ligand (R=H in the copper analogs of **1**) to copper(II) ions [42], while the coordination of the respective copper(I) [42] and yttrium (III) [43] complexes is essentially trigonal prismatic.

The observed Fe–N bond lengths (around 1.95 Å) indicate diamagnetic, low-spin iron(II) at 150 K. The significant divergence in bond lengths with respect to donor nature (*d*(Fe–N_{pyr}) – *d*(Fe–N_{aldimine}) = 6 pm) points to a non-isotropic ligand field around iron(II); aldimine N is an intrinsically stronger donor than pyridine N. We note, however, that the order of metal–N bond lengths is inverted in the related copper(I) and copper(II) complexes of Breher *et al.* [42].

3.2. Spectroscopic results for 1

3.2.1. Steady-state and dynamic UV/vis spectroscopy of 1. Well-resolved resonances in the ¹H NMR spectra of **1** at room temperature, with chemical shifts δ < 10 ppm and signal widths (full width at half maximum) below 2 Hz, are the typical signature of diamagnetic compounds. Accordingly, the UV/vis spectrum of **1** at room temperature in methanol shows the features typical of low-spin iron(II) complexes with polypyridyl ligands [44]. The

Table 2. Selected average bond lengths or inter-atomic distances (Å), angles (°), and trigonal torsions (°) for **1** with standard deviations in parentheses; for the sake of comparison, data for the phenol ether analog **2** [16] are also given.

	1	2
<i>(Mean) distances</i>		
<i>d</i> (Fe–N _{imin})	1.922(2)	1.915(2)
<i>d</i> (Fe–N _{pyr})	1.984(5)	1.974(3)
<i>d</i> (O···O)	5.8(3)	5.8(1)
<i>Angles</i>		
(N–Fe–N) _{trans}	166.9(8)	167.2(1)
Σ _{cis} ^a	51	61
θ ^b	44.3(5)	44.5(7)

^aSummed deviation from 90° of 12 *cis* angles.

^bTrigonal twist angle [31].

intense absorption bands in the range 400–600 nm with ϵ_{\max} approaching $10^4 \text{ M}^{-1} \text{ cm}^{-1}$ are assigned as $^1A_1 \rightarrow ^1\text{MLCT}$ transitions of **1** in its low-spin configuration (figure 2(a)). We notice a slight temperature dependence of the width of the metal–ligand charge transfer (MLCT) transitions of **1**. Area-conserving narrowing of the MLCT feature around 490 nm is accompanied by a slight red shift at lower temperatures ($\Delta\nu = 100 \text{ cm}^{-1}$ at 193 K; see figure S2, Supplementary Material). We attribute these minor temperature effects to diminished vibrational coupling of the electronic transition at lower temperature, rather than invoking effects of spin-state equilibria or varied speciation.

Starting with the pioneering work of McGarvey in the early 1980s [45], pulsed excitation of MLCT absorption bands in low-spin iron(II) complexes is now established as a selective way to populate metastable high-spin states [17–23, 46–48] (scheme 1). Accordingly, excitation of the MLCT transitions of **1** and **2** in acetonitrile, methanol, and water solutions



Scheme 1. Population of iron(II) quintet states via MLCT excitation.

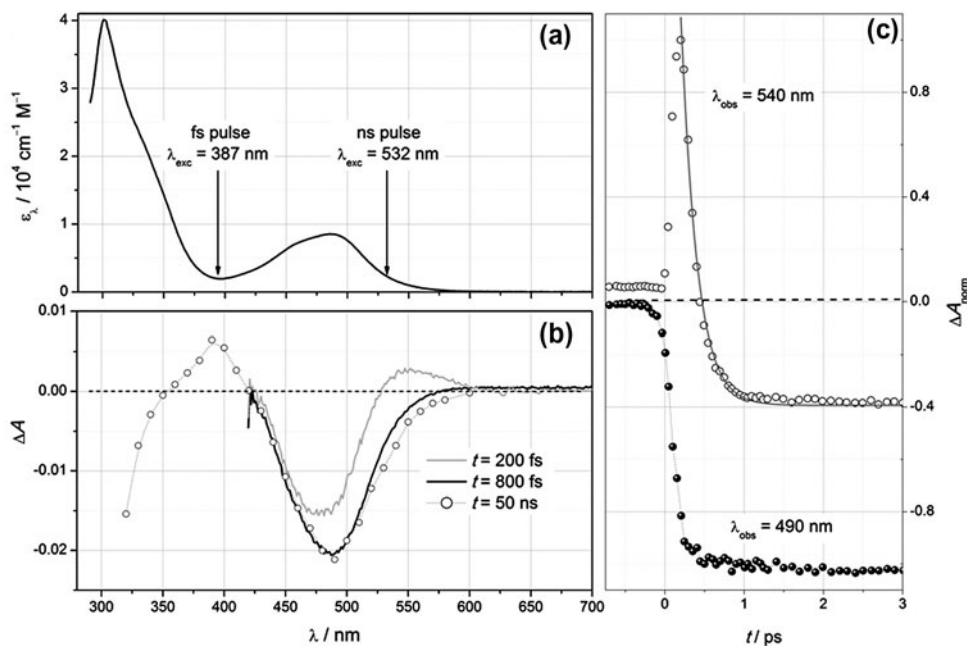


Figure 2. (a) UV/vis spectrum of **1** in MeOH solution (laser excitation wavelengths for pulsed irradiation are highlighted); (b) corrected transient absorption spectra obtained from CH_3CN solutions of **1** ($\text{OD}_{387} = 0.22$; full lines) at $t = 200 \text{ fs}$ (gray line) and $t = 800 \text{ fs}$ (black line) after laser excitation at 387 nm ($I_{\text{exc}} = 200 \text{ nJ}$; fwhm = 150 fs); open circles denote the transient absorption spectrum of **1** ($\text{OD}_{532} = 0.26$) at $t = 50 \text{ ns}$ after laser excitation at 532 nm ($I_{\text{exc}} = 2\text{--}3 \text{ mJ}$; fwhm = 8 ns); (c) normalized time profiles of recorded transient absorption at 520 nm (gray) and at 490 nm (black) after laser excitation of an acetonitrile solution of **1** at 387 nm ($I_{\text{exc}} = 200 \text{ nJ}$; fwhm = 150 fs); solid line: fit to a mono-exponential decay function.

has been used by us to study the dynamics of the population and depopulation of the corresponding high-spin states. In order to validate our observations, the study of **1** was supplemented by a time-resolved spectroscopic study of $[\text{Fe}\{\text{trenpy}_3\}](\text{BF}_4)_2$, whose spectral features and fs-dynamics have been documented in detail [49]. We note that our results for $[\text{Fe}\{\text{trenpy}_3\}](\text{BF}_4)_2$ closely reproduce these literature data.

Figure 2(b) highlights the early spectral evolution recorded for **1** between 200 and 800 fs after photoexcitation at 387 nm (full lines in figure 2(b); control experiments with ns time resolution at 355 and 532 nm proved the transients to be indifferent to the excitation wavelength). Clearly, the corrected transient spectrum recorded after 800 fs is dominated by a characteristic bleach of absorption around 490 nm that closely mimics the spectral shape of the ground-state absorption spectrum (figure 2(a)). This spectrum is indistinguishable from the spectral data recorded at $t = 50$ ns after excitation of **1** at 532 nm (symbols in figure 2(b)) and is therefore assigned as arising from the metastable high-spin state of **1**. Directly after fs-excitation ($t = 200$ fs in figure 2(b)), the bleach component in the spectrum around 490 nm, which is caused by ground-state depopulation, is convoluted with a second, much short-lived transient. This latter transient exhibits significant absorption, which is red shifted with respect to the ground-state chromophore. It is assigned as the MLCT state of **1**, by way of comparison with the spectral characteristics reported for iron(II) and ruthenium(II) polypyridyl complexes on this timescale [50–54].

The time profiles of transient absorption recorded at 520 nm and at 490 nm reflect the aforementioned early spectral evolution of excited **1** (figure 2(c)), and this is also closely mimicked by the phenol ether analog **2** (figure S3, Supplementary Material). A laser profile-limited rise of transient absorption at 520 nm and the accompanying laser profile-limited bleach at 490 nm is assigned as the population of the MLCT state of **1**. Depopulation of this transient is a very rapid process also. Mono-exponential fits of corrected transient decay yield apparent MLCT decay lifetimes of (172 ± 6) and (200 ± 5) fs for **1** and **2**, respectively. As these numbers are not significantly different from the excitation pulse width of 150 fs, the apparent lifetimes from the fits represent upper limits of the real MLCT-state lifetimes. Similar observations have been reported for a number of iron(II) complexes [50–54]. The residual bleach component that remains after the end of the ultrafast MLCT depopulation at $t = 1$ ps persists on the ns timescale. Its decay has been studied by means of ns-laser flash photolysis (see section 3.2.3.).

3.2.2. Spectroscopic titration of 1. Steady-state UV/vis spectra of dissolved **1** reveal the MLCT transitions in the visible to be largely independent of solvent effects (methanol, acetonitrile, and water). Spectral consistency persists throughout the time-resolved studies (see section 3.2.3.) and points to conserved compound speciation in different solvents. In particular, autoprotolysis of the complex-appended phenolic hydroxyl groups does not play a significant role.

Speciation of **1**, however, can be tuned in the presence of external bases as can be read from the steady-state UV/vis spectra at ambient temperature (figure 3) as a function of the added amount of potassium hydroxide in ethanol. Addition of aliquots of dissolved KOH causes two major spectral effects. First, a substantial red shift of the ligand-centered transitions in the near-UV is observed. Upon addition of one and two equivalents of base, the near-UV peak maximum shifts from 302 to 310 and 351 nm (figure 3(b)), respectively, overall by as much as 5000 cm^{-1} . We attribute the red-shifted absorption band to the $\pi \rightarrow \pi^*$ transition of the phenolate groups formed via deprotonation of the phenolic hydroxyl groups.

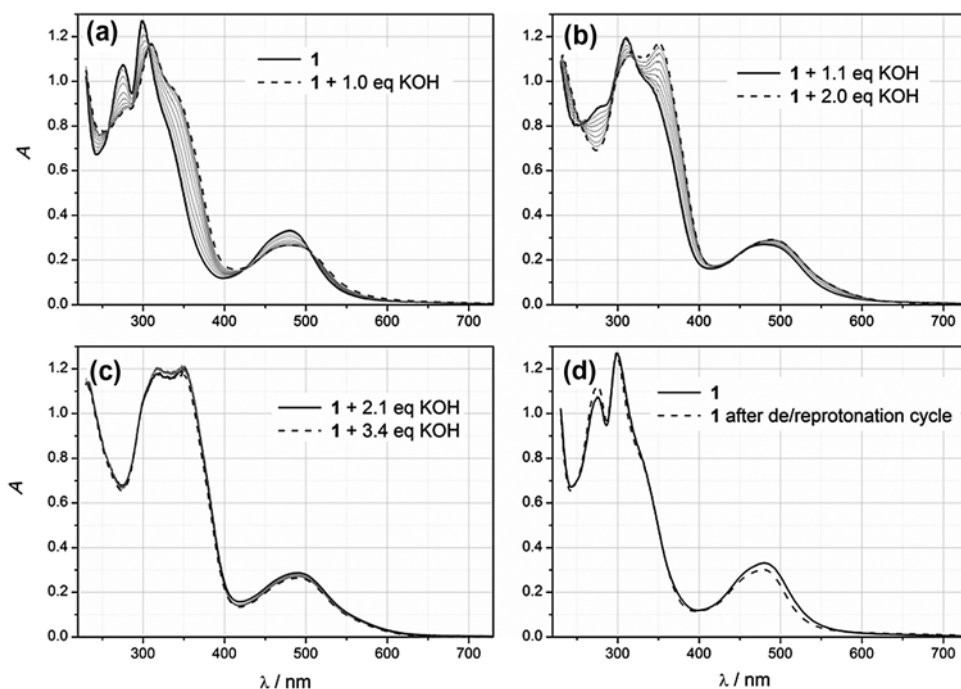


Figure 3. UV/vis spectroscopic titration of **1** in EtOH solution with KOH (a) up to 1.0 equivalents of KOH, (b) from 1.1 up to 2.0 equivalents of KOH, and (c) from 2.1 up to 3.4 equivalents of KOH; (d) UV/vis spectra of native **1** (full line) and of **1** recovered by back titration with aqueous HClO_4 (broken line).

Secondly, in the MLCT region, the base-induced red shift of the absorption maximum is less pronounced ($\Delta\nu = 600 \text{ cm}^{-1}$) than in the near-UV but, clearly, the deprotonation of appending phenol functions also affects the electron distribution within the $[\text{FeN}_6]$ core of the complex. The spectral changes give rise to well-defined isosbestic points (ip). Interestingly, we recorded two individual sets of isosbestic points during the titration. The first set of points ($\lambda_{\text{ip}} = 257/307/429/505 \text{ nm}$) is recorded during the addition of up to 1.0 equivalents of base, whereas the second set of points ($\lambda_{\text{ip}} = 257/321/457 \text{ nm}$) characterizes the spectral changes upon addition of 1.1 up to 2.0 equivalents of base. The occurrence of individual sets of isosbestic points indicates consecutive deprotonation steps with sharp speciation curves, *i.e.* after addition of 1.0 or 2.0 equivalents of base, the solution is strongly dominated by discrete complex species that have lost one or two of their acidic protons, respectively. The continued addition of further aliquots of KOH does not induce further changes neither in near-UV spectra nor in the MLCT region around 500 nm, where the spectral changes run into saturation after addition of two equivalents of base (figure 3(c)). Apparently, only two out of the three phenolic hydroxyl groups per complex molecule are readily deprotonated. The spectral changes upon base titration turned out to be fully reversible upon addition of a slight excess of aqueous HClO_4 (figure 3(d)).

Discontinuous addition of KOH to solutions of **1** in MeOH (figure 4(a)) reveals minor solvent-induced deviations in the near-UV absorption pattern but retains the base-driven spectral red shifts (see above) and, importantly, the saturation of spectral changes after addition of two equivalents of base. We conclude that the speciation of **1** is not affected by the

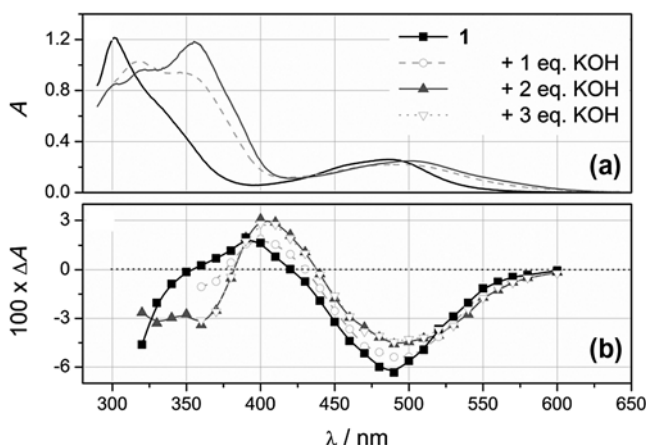


Figure 4. UV/vis spectroscopic titrations of **1** in MeOH solution with KOH; (a) steady-state absorption spectra of **1** and (b) transient absorption spectra recorded at $t = 60$ ns after laser excitation ($\lambda_{\text{exc}} = 532$ nm; $I_{\text{exc}} = 3$ mJ; fwhm = 9 ns) of **1** in MeOH after addition of n equivalents of KOH ($n = 0-3$).

nature of the alcohol. Base-driven red shifting of the MLCT feature is accompanied by significant broadening or tailing of the absorption band toward the NIR region, which is found to be reversed at lower temperature (see figure S4, Supplementary Material).

Pulsed excitation of the solutions of **1** in MeOH/KOH at 532 nm reveals that the base-driven red shift of the MLCT and of the near-UV ligand-centered absorption bands of **1** translates into a corresponding red shift of the bleach signal in the transient absorption spectra (figure 4(b)). Interestingly, changes of spectral appearance again saturate after addition of two equivalents of KOH, which points to an inert third phenolic hydroxyl function. We note, however, that addition of a substantial excess of base (*ca.* 20 eq) induces further changes in the transient spectra and the decay dynamics that may be ascribed to the third deprotonation step. We therefore conclude that titration of **1** with KOH yields complexes of distinct “protonation status” via successive deprotonation of the phenol functions in a stepwise manner that can be addressed optically and individually (figure 5). Notably, the “protonation status” of **1** directly affects the quintet-state lifetimes $\tau_{1 \leftarrow 5}$ (figure 5).

In both methanol and aqueous solution, the decay lifetimes are significantly shortened in the presence of KOH. For MeOH solution, the lifetimes of $^5[1(-aH)]$ are found to decrease by a factor of 3 with increasing degree of deprotonation (lifetimes in figure 5; time profiles for $a = 0$ and $a = 2$ in figure 6). Decay of transient absorption and bleach recovery can be ascribed to a single process in all cases. We assign this process as the singlet-state recovery of the protomers of **1**. The time profiles follow clean first-order kinetics without any long-lived spectral background, irrespective of wavelength and of base load. There is essentially no spectral evolution during the signal decay that would indicate changes of speciation of **1** during the excitation/relaxation cycle. As temperature scans have revealed, the differences in room temperature lifetimes are mainly due to differences in the thermal activation barriers of spin-state interconversion (see below).

Contrary to general experience, the kinetics of the decay process of native **1** is coupled to the solvent nature to a significant extent. While a lifetime of $\tau_{1 \leftarrow 5} = 440$ ns measured in water closely resembles the value found in MeOH, the lifetime of $\tau_{1 \leftarrow 5} = 950$ ns in

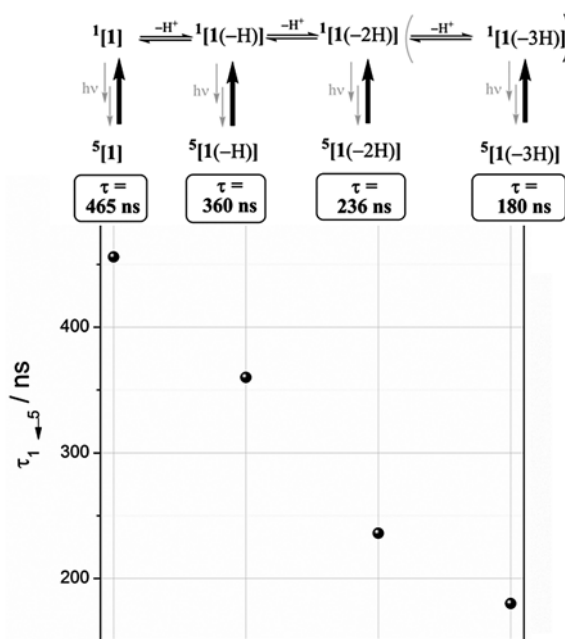


Figure 5. Speciation of **1** and room temperature, quintet-state lifetimes in MeOH in dependence of base-driven protolysis.

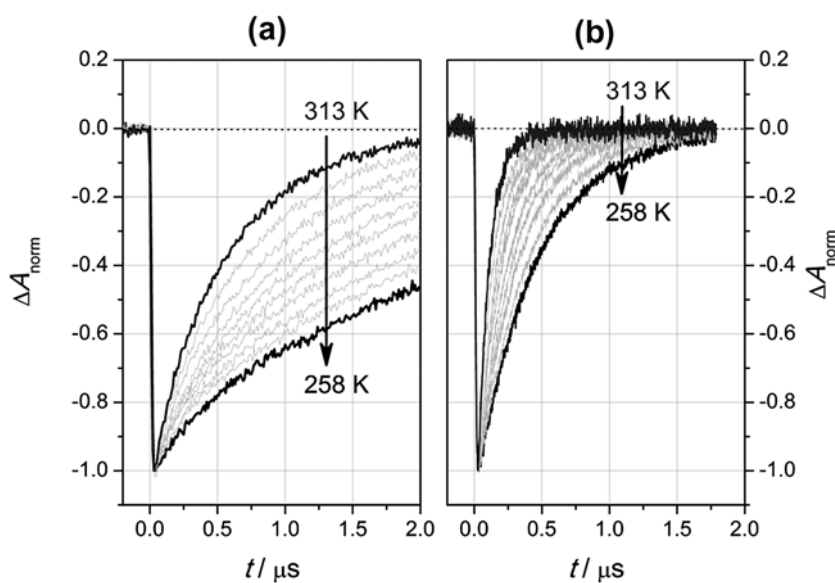


Figure 6. Decay profiles of transient absorption after laser excitation ($\lambda_{\text{exc}} = 532$ nm; $I_{\text{exc}} = 3$ mJ; fwhm = 9 ns) of **1** in MeOH (left panel) and of $1[1(-2H)]$ in MeOH (right panel) at variable temperatures.

acetonitrile points to a surprisingly strong influence of the solvent. A smaller solvent effect was found for both, the phenol ether **2** ($\tau_{1\leftarrow 5} = 700$ ns in MeOH; $\tau_{1\leftarrow 5} = 960$ ns in acetonitrile) and the pyridine-bearing parent compound of **1** ($R = H$ in figure 1; $\tau_{1\leftarrow 5} = 1700$ ns in MeOH; $\tau_{1\leftarrow 5} = 2100$ ns in acetonitrile [15]), both lacking hydroxyl groups. In consequence, kinetic divergence of **1** is attributed mainly to the presence of phenolic hydroxyl functions in **1** that take part in hydrogen-bonding phenomena of the solvent. This hydrogen-bonding effect on SCO kinetics parallels a report by Halcrow *et al.*, who has identified hydrogen-bonding of remote $>NH$ groups of iron(II) complexes to the solvent as an important parameter of the SCO thermodynamics [55].

3.2.3. Thermal barriers of high-spin relaxation. A previous analysis of the temperature dependence of the spin-state relaxation of **1** and three homo-topological analogs in MeOH has yielded thermal activation barriers (E_a ; Arrhenius model) [25] that had no precedent in the literature. In this work, we substantiate the activation parameters of **1** in detail, with respect to solvent nature and degree of base-driven protolysis.

As exemplified by experiments with **1** and [**1**(-2H)] in MeOH (see figure 6), the decays of the bleach recovery profiles of the species are strongly temperature dependent. Logarithmic plots of the decay rate constants $k_{1\leftarrow 5}$ (or of the decay lifetimes, $\tau_{1\leftarrow 5}$) against $1/T$ can be convincingly fitted within the Arrhenius model to yield the activation parameters. The data obtained for **1** are summarized in table 3. Compound **2** without protolysable groups supplies comparative data.

Two main features emerge from the summarized data. First, we note that the intercepts of the Arrhenius plots A_0 are, not only, largely indifferent with respect to the solvent, but they are also little affected by the status of the oxo-substituent of the pyridine rings in **1** or **2**. Neither deprotonation of the hydroxyl function of **1** nor its *O*-alkylation to yield **2** induce dynamics in A_0 exceeding a factor of 2.

Secondly, as we concluded earlier, diverging quintet-state decay kinetics of iron(II) complexes are largely ascribable to the variation in the thermal barriers, E_a , i.e. the variation in E_a in table 3 amounts to *ca.* 6 kJ mol⁻¹. This variation in E_a is of high significance. It should be discussed in relation to the *absolute* value of $E_a = 7$ kJ mol⁻¹, which was reported for [Fe{trenpy₃}] (PF₆)₂ [56]. While *O*-alkylated **2** and native **1** vary only little in their thermal barriers, significantly smaller barriers apply to the deprotonated species, presumably [**1**(-3H)], irrespective of solvent. We ascribe the base-driven decrease in the thermal barrier to an increase in driving force for ground-state recovery; that is, concomitant

Table 3. Arrhenius analysis^a of the quintet-state decays of **1** and **2**.

Species	Solvent	A_0 (10 ⁹ s ⁻¹)	E_a (kJ mol ⁻¹)
1	CH ₃ CN	3.6 ± 0.4	19.9 ± 0.3
1 ^b	MeOH	3.2 ± 0.4	18.0 ± 0.2
1	H ₂ O	2.8 ± 0.5	17.4 ± 0.4
1	MeOH/KOH ^c	3.8 ± 0.3	15.6 ± 0.2
1	H ₂ O/KOH ^c	3.8 ± 1.3	16.9 ± 0.7
2	CH ₃ CN	4.6 ± 0.4	21.1 ± 0.2
2	MeOH	5.3 ± 1.0	20.4 ± 0.3

^aEvaluated using: $\ln k_{HS} = \ln A_0 - E_a/RT$.

^bFrom Ref. [15]

^cExcess of KOH (*ca.* 20 eq.).

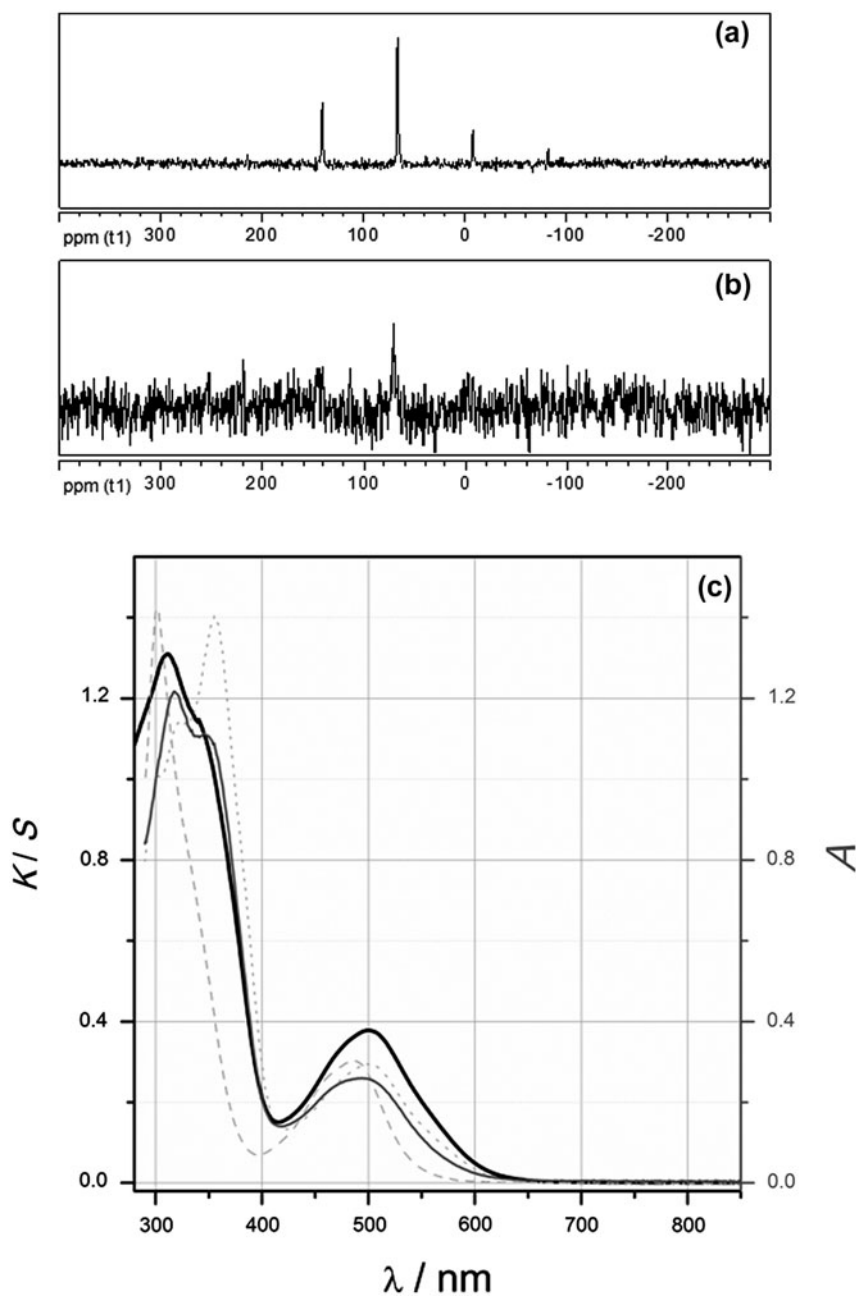


Figure 7. Spectroscopic characterization of surface-grafted **1** at Al_2O_3 ; ^{31}P -MAS-NMR spectra of bulk **1** (a) and **1** at Al_2O_3 (b); diffuse reflectance spectrum of surface-grafted **1** at Al_2O_3 ((c); black); for the sake of comparison, the solution UV/vis spectra of **1** in MeOH/KOH (n eq; gray) are replotted from figure 4 ($n = 0$: broken line; $n = 1$: bold line; $n = 2$: dotted line).

with deprotonation, the singlet ground state is stabilized. A similar stabilization of the singlet state via deprotonation of remote >NH groups of iron(II) complexes has been reported by Jameson *et al.* [57].

3.3. Surface grafting of **1** to alumina: **1** at Al₂O₃

As described in the preceding sections, **1** and **2** exhibit a highly hindered spin-state inter-conversion. While the molecular reasons for the extreme behavior of **1**, **2** and of their homo-topological congeners are the subject of an ongoing investigation, the persistence of their excited state makes these compounds particularly interesting candidates for surface deposition studies. In a preceding study, we found that the *O*-alkylated compound **2** is labile on gold surfaces [26]. Fragmentation of the ligand backbone is the likely reason for irreversible reactions of the P(S)N₃ capping unit. By contrast, **1** has been found in the present study to adsorb readily to hydrous metal oxide surfaces from solution, while retaining its molecular integrity.

Surface grafting of **1** to alumina was accomplished by a wet impregnation technique. Slurries of alumina in acetone were treated with **1** and left stirring for 30–90 min. During this period, the solution phase gradually faded in color, while the solid took on an intense pink color (similar observations apply to grafting of **1** on titania and silica). The complex-loaded oxide powder, **1** at Al₂O₃, was separated from solution by filtration. Importantly, treatment of the residue with excess acetone did not induce complex leaching. After drying in a vacuum, **1** at Al₂O₃ was characterized by means of diffuse-reflectance UV/vis spectroscopy and ³¹P-MAS-NMR spectroscopy of powder samples.

Diffuse reflectance spectra of the metal-loaded material (see figure 7(c)) are consistent with our formulation as a composite material, **1** at Al₂O₃. The main chromophores of **1** in the near-UV and the visible regions are conserved on the oxide surface. Comparison with the solution-phase spectra of **1** points to some degree of spontaneous protolysis of the phenol groups on alumina. The spectra of **1** at Al₂O₃ are best matched with the spectra of **1** in MeOH in the presence of 1 equivalent of KOH, that is, with what likely is [**1**(–H)]. Phenolic hydroxyl groups are known to undergo spontaneous protolysis, if adsorbed on oxide surfaces [17]. The ³¹P-MAS-NMR spectrum of **1** at Al₂O₃ (figure 7(b)) suggests the presence of a single phosphorous-containing species on the alumina surface. The chemical shift matches the bulk parent complex **1** (figure 7(a)) closely, suggesting that the chemical environment of the phosphorous atom of the grafted species is nearly identical to the parent complex.

4. Conclusion

In this work, we addressed the photo-induced spin-state dynamics of the low-spin iron(II) complex **1** with appended protolysable groups. On irradiation of solutions of **1** with UV/vis light, the (trigonally) distorted octahedral singlet ground state, which has been identified by ¹H NMR and steady-state UV/vis spectroscopies and structurally characterized by X-ray structure analysis, yields a long-lived, high-spin state via an ultrafast relaxation cascade. Hydrogen bonding to the solvent is identified as an important control factor of decay kinetics of the parent complex **1**. The spectral appearance of the singlet ground state and the

decay kinetics of the excited quintet state, respectively, were susceptible to the presence of external bases. Deprotonation of the appended phenol functions of **1** in solution progressively stabilizes the singlet ground state and favors enhanced ground-state recovery.

Partial protolysis of the phenol groups of **1** accompanies surface grafting from solutions of **1** on hydrous metal oxide powders. While deeper insights into the molecular mechanism of adsorption of **1** and its structure on the surface are subjects of ongoing work [58], the conserved UV/vis chromophore and the conserved ^{31}P -NMR resonance of **1** at Al_2O_3 point to retained integrity of the complex. We conclude that surface grafting of phenol-bearing metal complexes from solution provides a straightforward method to immobilize functional metal complexes on metal oxide surfaces. The ready access to immobilized, *salt-like* metal complexes may find broader application in the field of heterogenized SCO research.

Supporting information

Hydrogen-bonding pattern of the hydroxyl groups of **1** in the solid state (figure S1), variable temperature, steady-state UV/vis spectra of **1** (figure S2), and [**1**(–2H)] (figure S3); sub-ps decay profile of transient absorption of **2** (figure S4). CCDC-1054327 contains the supplementary crystallographic data for this paper. These data can be obtained free of charge from the Cambridge Crystallographic Data Center via http://www.ccdc.cam.ac.uk/data_request/cif.

Acknowledgements

Support of this work by the Deutsche Forschungsgemeinschaft (SFB 658, “Elementary processes in molecular switches on surfaces”) is gratefully acknowledged. Professor Dr Thorsten Ressler (Technische Universität Berlin) is thanked for assistance with diffuse reflectance spectroscopy. G.H. thanks Professor Dr Dirk Guldi (Friedrich-Alexander-Universität Erlangen-Nürnberg) for providing access to the fs-LFP facilities and Professor Dr Bronisław Marciniak and Dr Tomasz Pedziński (Adam Mickiewicz University Poznań) for continuous support and assistance with ns-LFP photolysis.

Disclosure statement

No potential conflict of interest was reported by the authors.

References

- [1] M.A. Halcrow (Ed.). *Spin-crossover Materials: Properties and Applications*, John Wiley & Sons, Chichester (2013).
- [2] M.A. Halcrow. *Chem. Soc. Rev.*, **40**, 4119 (2011).
- [3] C. Lochenie, W. Bauer, A.P. Railliet, S. Schlamp, Y. Garcia, B. Weber. *Inorg. Chem.*, **53**, 11563 (2014).
- [4] S. Heider, H. Petzold, G. Chastanet, S. Schlamp, T. Rüffer, B. Weber, J.-F. Létard. *Dalton Trans.*, **42**, 8575 (2013).
- [5] O. Kahn, C. Jay Martinez. *Science*, **279**, 44 (1998).

- [6] A. Bousseksou, G. Molnár, L. Salmon, W. Nicolazzi. *Chem. Soc. Rev.*, **40**, 3313 (2011).
- [7] P. Gütllich, A.B. Gaspar, Y. Garcia. *Beilstein J. Org. Chem.*, **9**, 342 (2013).
- [8] S. Brooker. *Chem. Soc. Rev.*, **44**, 2280 (2015). doi: [10.1039/C4CS00376D](https://doi.org/10.1039/C4CS00376D).
- [9] P. Gütllich, H.A. Goodwin, M.-L. Boillot. *Top. Curr. Chem.*, **234**, 261 (2004).
- [10] M. Milek, F.W. Heinemann, M.M. Khusniyarov. *Inorg. Chem.*, **52**, 11585 (2013).
- [11] S. Venkataramani, U. Jana, M. Dommaschk, F.D. Sönnichsen, F. Tuczek, R. Herges. *Science*, **331**, 445 (2011).
- [12] M. Dommaschk, M. Peters, F. Gutzeit, C. Schütt, C. Nähter, F.D. Sönnichsen, S. Tiwari, C. Riedel, S. Boretius, R. Herges. *J. Am. Chem. Soc.*, **137**, 7552 (2015). doi: [10.10231/jacs.5b00929](https://doi.org/10.10231/jacs.5b00929).
- [13] S. Decurtins, P. Gütllich, C.P. Köhler, H. Spiering, A. Hauser. *Chem. Phys. Lett.*, **105**, 1 (1984).
- [14] J.-F. Létard, L. Capes, G. Chastanet, N. Moliner, S. Létard, J.-A. Real, O. Kahn. *Chem. Phys. Lett.*, **313**, 115 (1999).
- [15] A. Hauser, C. Enachescu, M. Lawson Daku, A. Vargas, N. Amstutz. *Coord. Chem. Rev.*, **250**, 1642 (2006).
- [16] J. Klingele, D. Kaase, M. Schmucker, Y.H. Lan, G. Chastanet, J.-F. Létard. *Inorg. Chem.*, **52**, 6000 (2013).
- [17] J.K. McCusker, K.N. Walda, R.C. Dunn, J.D. Simon, D. Magde, D.N. Hendrickson. *J. Am. Chem. Soc.*, **114**, 6919 (1992).
- [18] W. Gawelda, A. Cannizzo, V.-T. Pham, F. van Mourik, C. Bressler, M. Chergui. *J. Am. Chem. Soc.*, **129**, 8199 (2007).
- [19] A.J. Conti, C.-L. Xie, D.N. Hendrickson. *J. Am. Chem. Soc.*, **111**, 1171 (1989).
- [20] S.K. Hain, F.W. Heinemann, K. Gieb, P. Müller, G. Hörner, A. Grohmann. *Eur. J. Inorg. Chem.*, 221 (2010).
- [21] C.-L. Xie, D.N. Hendrickson. *J. Am. Chem. Soc.*, **109**, 6981 (1987).
- [22] J.K. McCusker, H. Toftlund, A.L. Rheingold, D.N. Hendrickson. *J. Am. Chem. Soc.*, **115**, 1797 (1993).
- [23] A.H.R. Al-Obaidi, K.B. Jensen, J.J. McGarvey, H. Toftlund, B. Jensen, S.E.J. Bell, J.G. Carroll. *Inorg. Chem.*, **35**, 5055 (1996).
- [24] J.K. McCusker, A.L. Rheingold, D.N. Hendrickson. *Inorg. Chem.*, **35**, 2100 (1996).
- [25] P. Stock, T. Pedziński, N. Spintig, A. Grohmann, G. Hörner. *Chem. Eur. J.*, **19**, 839 (2013).
- [26] P. Stock, A. Erbe, M. Buck, D. Wiedemann, H. Ménard, G. Hörner, A. Grohmann. *Z. Naturforsch.*, **69b**, 1164 (2014).
- [27] W. Macyk, K. Szaciłowski, G. Stochel, M. Buchalska, J. Kuncewicz, P. Łabuz. *Coord. Chem. Rev.*, **254**, 2687 (2010).
- [28] M. Cavallini, I. Bergenti, S. Milita, G. Ruani, I. Salitros, Z.-R. Qu, R. Chandrasekar, M. Ruben. *Angew. Chem. Int. Ed.*, **47**, 8596 (2008).
- [29] M. Cavallini. *Phys. Chem. Chem. Phys.*, **14**, 11867 (2012).
- [30] A. Grohmann, M. Haryono, K. Student, P. Müller, M. Stocker. *Eur. J. Inorg. Chem.*, 662 (2013).
- [31] M. Bernien, D. Wiedemann, C.F. Hermanns, A. Krüger, D. Rolf, W. Kroener, P. Müller, A. Grohmann, W. Kuch. *J. Phys. Chem. Lett.*, **3**, 3431 (2012).
- [32] B. Warner, J.C. Oberg, T.G. Gill, F. El Hallak, C.F. Hirjibehedin, M. Serri, S. Heutz, M.-A. Arrio, P. Saintcivie, M. Mannini, G. Poneti, R. Sessoli, P. Rosa. *J. Phys. Chem. Lett.*, **4**, 1546 (2013).
- [33] T.G. Gopakumar, F. Matino, H. Naggert, A. Bannwarth, F. Tuczek, R. Berndt. *Angew. Chem. Int. Ed.*, **51**, 6262 (2012).
- [34] T. Miyamachi, M. Gruber, V. Davesne, M. Bowen, S. Boukari, L. Joly, F. Scheurer, G. Rogez, T.K. Yamada, P. Ohresser, E. Beaurepaire, W. Wulfhekel. *Nat. Commun.*, **3**, 938 (2012).
- [35] T.G. Gopakumar, M. Bernien, H. Naggert, F. Matino, C.F. Hermanns, A. Bannwarth, S. Mühlenberend, A. Krüger, D. Krüger, F. Nickel, W. Walter, R. Berndt, W. Kuch, F. Tuczek. *Chem. Eur. J.*, **19**, 15702 (2013).
- [36] P. Kubelka, F. Munk. *Z. Techn. Phys.*, **12**, 593 (1931).
- [37] R.C. Clark, J.S. Reid. *Acta Crystallogr.*, **A51**, 887 (1995).
- [38] G.M. Sheldrick. *Acta Crystallogr.*, **A64**, 112 (2008).
- [39] L.J. Farrugia. *J. Appl. Crystallogr.*, **30**, 565 (1997).
- [40] T. Pedzinski, A. Marciewicz, B. Marciniak. *Res. Chem. Intermed.*, **35**, 497 (2009).
- [41] M. Marchivie, P. Guionneau, J.-F. Létard, D. Chasseau. *Acta Cryst.*, **61**, 25 (2005).
- [42] I. Trapp, M.W. Löble, J. Meyer, F. Breher. *Inorg. Chim. Acta*, **374**, 373 (2011).
- [43] M.W. Löble, M. Casimiro, D.T. Thielemann, P. Oña-Burgos, I. Fernández, P.W. Roesky, F. Breher. *Chem. Eur. J.*, **18**, 5325 (2012).
- [44] E.C. Constable, G. Baum, E. Bill, R. Dyson, R. van Eldik, D. Fenske, S. Kaderli, D. Morris, A. Neubrand, M. Neuburger, D.R. Smith, K. Wieghardt, M. Zehnder, A.D. Zuberbühler. *Chem. Eur. J.*, **5**, 498 (1999).
- [45] J.J. McGarvey, I. Lawthers. *J. Chem. Soc., Chem. Commun.*, 906 (1982).
- [46] C. Brady, J.J. McGarvey, J.K. McCusker, H. Toftlund, D.N. Hendrickson. *Top. Curr. Chem.*, **235**, 1 (2004).
- [47] P. Gütllich. *Top. Curr. Chem.*, **234**, 155 (2004).
- [48] O. Sato, J. Tao, Y.-Z. Zhang. *Angew. Chem. Int. Ed.*, **46**, 2152 (2007).
- [49] A.L. Smeigh, M. Creelman, R.A. Mathies, J.K. McCusker. *J. Am. Chem. Soc.*, **130**, 14105 (2008).
- [50] J.K. McCusker. *Acc. Chem. Res.*, **36**, 876 (2003).
- [51] W. Gawelda, A. Cannizzo, V.-T. Pham, F. van Mourik, C. Bressler, M. Chergui. *J. Am. Chem. Soc.*, **129**, 8199 (2007).

- [52] E. Amouyal, M. Bahout, G. Calzaferri. *J. Phys. Chem.*, **95**, 7641 (1991).
- [53] A. Cannizzo, C.J. Milne, C. Consani, W. Gawelda, C. Bressler, F. van Mourik, M. Chergui. *Coord. Chem. Rev.*, **254**, 2677 (2010).
- [54] S. Szalis, C. Consani, A. El Nahhas, A. Cannizzo, M. Chergui, F. Hartl, A. Vlcek. *Inorg. Chim. Acta*, **374**, 578 (2011).
- [55] S.A. Barrett, C.A. Kilner, M.A. Halcrow. *Dalton Trans.*, **40**, 12021 (2011).
- [56] A. Hauser, A. Vef, P. Adler. *J. Chem. Phys.*, **95**, 8710 (1991).
- [57] M. Emanulla, W. Linert, V. Gutmann, R.F. Jameson. *Monatsh. Chem.*, **125**, 1301 (1994).
- [58] Y. Tong, N. Spintig, K. Campen, G. Hörner. Unpublished results.